Opt Quant Electron (2015) 47:1949–1963
DOI 10.1007/s11082-014-0062-5

Hybrid III–V semiconductor/silicon three-port filter on 1D-PhC wire

Stefania Malaguti · Gaetano Bellanca · Alexandre Bazin · Fabrice Raineri · Rama Raj · Stefano Trillo

Received: 22 April 2014 / Accepted: 1 November 2014 / Published online: 9 November 2014

Abstract We report on the design of a hybrid III/V semiconductor/silicon three-port channel drop filter at 1,550 nm. The device is excited through a *Si* photonic wire positioned below the resonant cavity, which is in turn designed by properly drilling holes on a *InP* 1D-PhC wire. The output signal is collected by a photonic wire waveguide, laterally coupled to the resonator and terminated with a suitable mirror. To raise the drop efficiency above the theoretical limit of 50 % allowed by a design exploiting a single cavity, a different topology based on a two-cavity configuration is then investigated. In this case, a drop efficiency close to 100 % is obtained.

Keywords Photonic wires · Optical resonators · Wavelength filtering devices

1 Introduction

In this paper we present numerical results on the design of a 1D-PhC wire three-port filter for an integrated hybrid III–V semiconductor/silicon technology. Hybrid technology is an extremely promising solution for upcoming photonic circuits, as it combines the optoelectronic properties of III–V materials with CMOS compatibility. This technology has allowed the demonstration of many kinds of devices such as lasers (Campenhout et al. 2007), amplifiers (Park et al. 2007), and optical flip-flops (Thourhout et al. 2010). At the same time photonic crystals (PhCs), owing to their fundamental properties (Notomi 2010), are considered to be promising building blocks for high-density photonic integrated circuits. Extremely

S. Malaguti · G. Bellanca (✉) · S. Trillo
Department of Engineering, University of Ferrara, Ferrara, Italy
e-mail: gaetano.bellanca@unife.it

S. Malaguti
e-mail: stefania.malaguti@unife.it

A. Bazin · F. Raineri · R. Raj
Laboratoire de Photonique et de Nanostructures, CNRS-UPR20, Marcoussis, France

compact PhC microcavity filters for optical communications have been proposed and demonstrated in the literature, such as add-drop filters (Qiang et al. 2007), channel drop filters (Wang and Chen 2010; Niemi et al. 2006; Nguyen et al. 2013), and bandpass filters (Chao et al. 2007). PhC cavities have also shown their capacity to provide both small size and high nonlinear response (Combrié et al. 2013). All-optical switching has been recently demonstrated using an InP over SOI PhC nanocavity and the integration of a PhC nanolaser on top of SOI waveguides, confirming the potential of this hybrid technology for the fabrication of nanophotonic components (Halioua et al. 2011).

The paper is organized as follows: in the first section, the operation and the characteristics of the single-channel drop filter are summarized. Then, optimizations procedures for the design of the resonator and both the access and the drop waveguides are illustrated. Results relevant to a single cavity configuration conclude the first part of the paper. A different filter configuration, which exploits two resonant cavities to increase the drop efficiency of the device, is then proposed. Results are reported and discussed in the last section. Conclusions are drawn at the end.

2 Design of building blocks in the channel drop filters

The schematic top view of the proposed configuration for the investigated channel drop filter (CDF) is shown in Fig. 1. This topology is the transposition on the 1D-PhC wire technology of the well-known configurations proposed for devices made with 2D photonic crystal membranes (Shinya et al. 2006; Malaguti et al. 2013) and is similar to the one proposed in Veerasubramanian et al. (2012). With respect to this paper, originated by the pioneering work of Haus and Lai (1991, 1992), in our configurations the cavities are formed with holes drilled on the photonic wire waveguides, instead of using quarter-wave shifted sidewalled gratings. Moreover, we propose a design with hybrid technology.

The key device of this component is the resonant cavity, which is evanescently-coupled with both the bus and the drop waveguides. The bus is located below the cavity, and is vertically coupled with it. The drop waveguide, on the contrary, lies on the same horizontal plane of the resonator, and is laterally coupled with the cavity. On one side, this waveguide is terminated by a suitable positioned mirror, thus enabling the design of an efficient three-port filter.

As explained in the introduction, the proposed device is built on a hybrid III–V semiconductor/silicon technology. Therefore, components located on different vertical layers are built with distinct materials. Figure 2 shows the side view of the structure, where the position of each layer is highlighted.

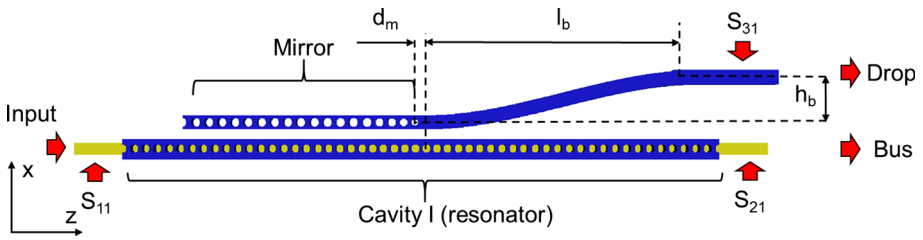

Fig. 1 *Top view* of the investigated structure. The bus waveguide (in *yellow*) is vertically coupled with the cavity, whereas the drop waveguide is laterally coupled with the resonator. To obtain a three-port device and increase the drop efficiency of the filter, a suitably positioned mirror on one side of the drop waveguide is considered in the design. (Color figure online)

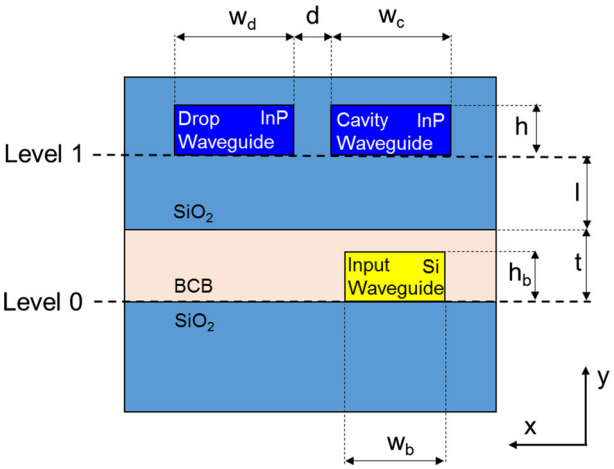

Fig. 2 Side view of the hybrid III–V device. The *Si* input waveguide (in *yellow*) lies on the *top* of a SiO_2 substrate at Level 0. On the contrary, the cavity and the drop waveguide (in *dark blue*) are positioned at Level 1 and enclosed on the second SiO_2 layer. Both of these components are made of *InP*. The second SiO_2 layer is grown above the BCB (*light red block* in the picture) which overlays the *Si* input waveguide. (Color figure online)

The bus is a Silicon wire waveguide (yellow block in Fig. 2, refractive index $n_{Si} = 3.47$) grown on the bottom level (indicated as Level 0 in the same picture) of the device. This photonic wire, whose width and thickness are respectively $w_b = 400\,\text{nm}$ and $h_b = 220\,\text{nm}$, lies on the top of a Silica (SiO_2) substrate (light blue blocks in Fig. 2, refractive index $n_{SiO_2} = 1.45$) and is fully embedded with Benzocyclobutene (BCB). BCB is a polymer widely used for microelectronic packaging and interconnect applications (Frear 1999; Liu et al. 1995). In the last years, however, BCB polymers have been recognized as attractive materials for both the development of hybrid optical technology and the realization of optical passive devices (Carette et al. 2008; Kane and Krchnavek 1995); thermal stability over 350 °C, good adhesion to most semiconductors, easy device fabrication and compatibility with planar PIC processing, in facts, make BCB well suited for optics and, in particular, for III–V semiconductor hybrid integration, where typically structures are grown layer-by-layer and require all the layers to be completely sealed (Zheng et al. 2004). In the proposed device configuration, the thickness of the BCB cladding has been set to $t = 300\,\text{nm}$. Its refractive index is $n_{BCB} = 1.537$.

Unlike the bus waveguide, the resonator and the drop are located at the Level 1 of the device (dark blue blocks in Fig. 2) and embedded with SiO_2 grown above the planarized BCB substrate. These two components are realized on a $h = 260\,\text{nm}$ *InP* layer positioned above the BCB layer. The refractive index of *InP* has been assumed to be $n_{InP} = 3.17$. The design and the optimization of this device have been performed with the same proprietary 3D-FDTD simulator used in Malaguti et al. (2013). Resonances and quality factors have been evaluated by post-processing 3D-FDTD time-domain data using Harminv from MIT (http://ab-initio.mit.edu/wiki/index.php/Harminv).

2.1 Design and optimization of the resonant cavity

The resonator used in the filter is a Fabry–Perot type cavity formed in a single mode *InP* wire waveguide (width $w_c = 650\,\text{nm}$, height $h_b = 220\,\text{nm}$) limited on both sides by high reflectivity mirrors constituted by a single row of $N_h = 2N$ holes drilled into the nanowire.

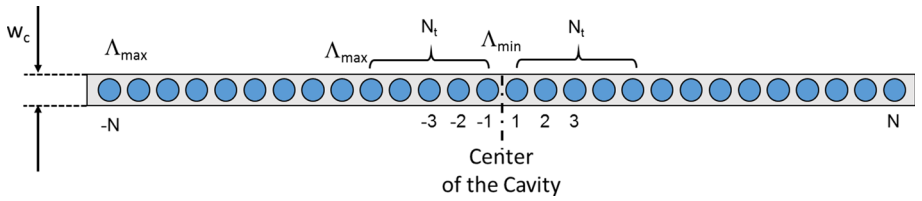

Fig. 3 Schematic representation of the 1D PhC cavity realized on the *InP* based photonic wire. Holes have a radius $r = 120$ nm. Waveguide width is $w_c = 650$ nm. The distance between the holes varies from Λ_{min} to Λ_{max} in the tapering regions of N_t holes positioned on each side of the cavity. Outside these tapering regions, holes are at the constant distance Λ_{max}

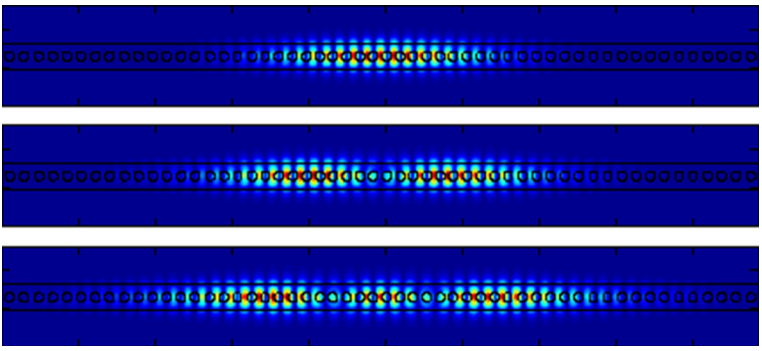

Fig. 4 Patterns of the transverse $| E_x |$ field component for the three cavity resonances on a horizontal xz plane positioned in the middle of the cavity. *Top* $\lambda_0 = 1{,}552$ nm, $Q_0 = 2.20 \times 10^7$. *Center* $\lambda_1 = 1{,}583$ nm, $Q_1 = 3.71 \times 10^5$. *Bottom* $\lambda_2 = 1{,}612$ nm, $Q_2 = 4.58 \times 10^4$

Investigations on these kind of cavities are described in Zain et al. (2008), Deotare et al. (2009), Zhang et al. (2010) and Ahn et al. (2010).

In our design, as in Halioua et al. (2010), the radius of the holes is kept fixed. Also the distance between adjacent holes is constant, except for the tapering regions (N_t holes, with $N_t < N$) located on both sides of the Fabry–Perot cavity, where the hole separation follows a Gaussian apodization. The geometry of the resonator is sketched in Fig. 3. The holes radius r and the variable pitch Λ_i of the 1D lattice have been optimized to obtain a large bandwidth of high reflectivity in the C-band (1,550 nm), thus increasing the quality of the Fabry–Perot resonator. Optimization through 3D-FDTD allowed us to obtain a resonance with the higher quality factor Q ($Q_0 = 2.20 \times 10^7$) at $\lambda_0 = 1{,}552$ nm with the following set of parameters: overall number of holes $N_h = 2N = 54$, number of holes in the tapering section $N_t = 6$, minimum and maximum values of the pitch respectively $\Lambda_{min} = 346$ nm and $\Lambda_{max} = 370$ nm. Other modes of the cavity at $\lambda_1 = 1{,}583$ nm and $\lambda_2 = 1{,}612$ nm have lower quality factors ($Q_1 = 3.71 \times 10^5$ and $Q_2 = 4.58 \times 10^4$, respectively) and are not interesting for the realization of filters with high selectivity. The patterns of the transverse $| E_x |$ field component for these three resonances on a horizontal xz plane positioned in the middle of the cavity are illustrated in Fig. 4.

In this section we have optimized the design of a Fabry–Perot cavity with resonant wavelength in the C-band, a free spectral range of 31 nm and very high quality factor. The overall length of the cavity is of about 20 nm, suggesting the possibility to fabricate devices at micrometer scale.

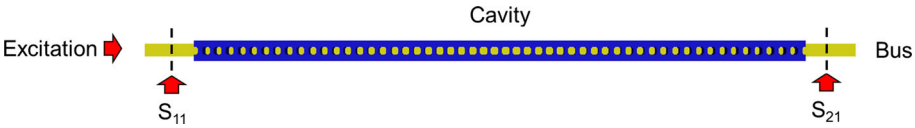

Fig. 5 Sketch of the simplified structure used to evaluate the coupling between the cavity and the bus. In this configuration, the drop waveguide has been completely removed from the simulated scenario

Table 1 Resonant frequencies λ_0 and quality factors Q_b of the fundamental mode of the 1D PhC cavity for values of the thickness l of the SiO_2 layer

l	λ(nm)	Q_b
350	1,557	2,200
400	1,558	3,600
450	1,558	6,200
500	1,558	14,000

2.2 Design and optimization of the bus waveguide

Once determined the effective parameters of the cavity, the coupling between the resonator and the bus waveguide should be optimized. Coupling between these two structures is a fundamental parameter for the final performance of the device, as it affects the bandwidth of the filter through the modification induced on the quality factor. To evaluate this parameter, the Q factor at the resonance as a function of the distance between the Si waveguide and the cavity has been computed. In this case the simplified structure illustrated in Fig. 5, where the drop waveguide has been completely removed from the simulated scenario, has been used.

The structure has been excited on the left side with a pulse signal having a suitable spectrum and the profile of the fundamental mode of the bus waveguide. As previously stated, the evaluation of the Q factor has been performed by post-processing with Harminv (http://ab-initio.mit.edu/wiki/index.php/Harminv) the time-domain evolution of the electric field collected by a field-probe positioned inside the resonator. Although the Q of the fundamental mode of the isolated cavity is very high ($Q_0 = 2.20 \times 10^7$), its value significantly drops due to the coupling. The coupled quality factor Q_b can be tuned by modifying the thickness l of the SiO_2 buffer layer positioned between the Si wire of the bus and the cavity, as shown in Table 1. As one can observe, while the resonance barely changes, the coupled quality factor Q_b is strongly affected by the values of l.

For this configuration it is interesting to plot the field patterns for different values of the wavelength. Figure 6 shows the patterns of the $|E_x|$ field component on a vertical yz plane positioned in the middle section of the cavity and the bus waveguide for three different wavelengths. The top picture refers to $\lambda = 1{,}552$ nm, which is the resonance of the cavity with the higher Q, whereas the image in the center corresponds to $\lambda = 1{,}566$ nm. For this wavelength no resonance exists, and the bus does not couple with the cavity; the field, in fact, flows unperturbed through the waveguide, as shown by the uniform color pattern. The figure on the bottom corresponds to $\lambda = 1{,}582$ nm; in this case, the cavity is excited by the mode with a low Q. This mode is not suitable for filtering, as the corresponding bandwidth is not sufficiently small.

In summary, a suitable bus waveguide for the previously configured Fabry–Perot cavity has been designed. By changing the distance between the resonator and the bus, a small deviation of the resonant frequency of the fundamental mode has been observed. The quality factor, on the contrary, is very sensitive to the coupling conditions, which can be modified

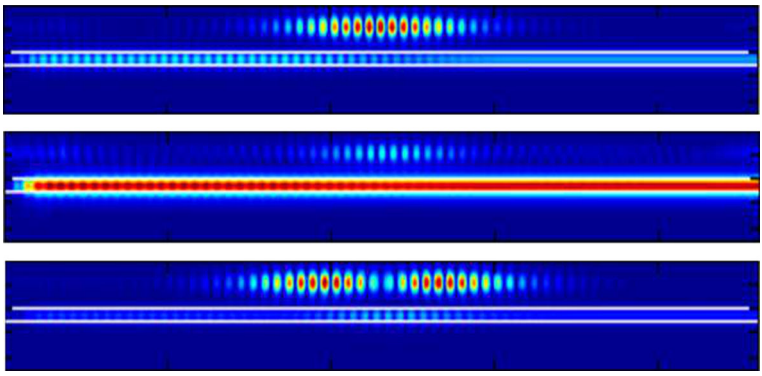

Fig. 6 Patterns of the $| E_x |$ field component for the three different wavelengths on the vertical yz plane cutting the cavity in the central section. *Top* $\lambda = 1{,}552$ nm (resonance of the cavity with the higher Q). *Center* $\lambda = 1{,}566$ nm (cavity out of resonance). *Bottom* $\lambda = 1{,}582$ nm (resonance of the cavity with a low Q)

by tuning the distance between the cavity and the bus waveguide. The optimization of this parameter will be fundamental for the bandwidth of the CDF.

2.3 Design and optimization of the drop waveguide

The next step of the design procedure of the CDF is the optimization of the coupling between the resonator and the drop waveguide. In this case, the coupling with the cavity should be tuned in order to satisfy the condition of the maximum power transfer toward the drop described in Ren et al. (2006). This condition requires that $Q_b/Q_d = 2$, being Q_b and Q_d the quality factors of the resonator (Cavity I in Fig. 1) related to the rate of decay into the bus and drop waveguides respectively. In order to satisfy this constraint, different configurations have been simulated and the corresponding values of Q_d have been computed through the same procedure described in the previous section (except for the position of the excitation, now introduced on the drop waveguide). Both the width of the photonic wire w_d and the distance from the cavity d could be used as design parameters. However, to avoid technological problems in the realization of the device that could occur if the gap d between waveguide and cavity is too small, the distance between the resonator and the drop has been chosen as $d = 300$ nm. In this condition, the coupled quality factor Q_d of the cavity follows, as a function of the waveguide width w_d, the trend reported in Fig. 7.

This section describes the optimized design of the drop waveguide. In this procedure, the width of the waveguide and the distance from the Fabry–Perot cavity play an important role, as both define the quality factor (and therefore the bandwidth) of the filter. For a distance $d = 300$ nm between waveguide and cavity (chosen to avoid problems in the technological process), the trend of the quality factor has been determined by simulations. These results, as explained in the next section, will be used to design the CDF with the desired bandwidth and the maximum drop efficiency.

2.4 Design and optimization of the waveguide bend

Another important component of the filter to be optimized is the waveguide bend, which is used to turn away the drop waveguide from the resonator after the coupling section. Waveguide bend is not strictly needed when a topology based on a single cavity (see Fig. 1)

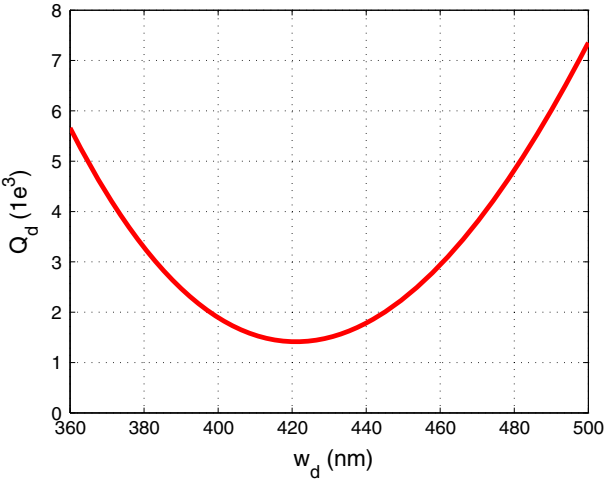

Fig. 7 Quality factor of the resonator Q_b when loaded with the drop as a function of the waveguide width w_d. These values have been obtained for a gap between the drop and the cavity $d = 300$ nm

is considered. However, when also a second cavity acting as a mirror is introduced in the configuration of the filter (see Fig. 13), bending of the drop is mandatory. The bend in fact, by turning away the drop waveguide, removes the undesired coupling with the second cavity (Cavity II).

In our configuration, a *S-bend* with a sinusoidal profile has been used. Important parameters for this structure are the length l_b and the lateral shift h_b with respect to the straight path (see the sketch illustrated on the top panel of Fig. 8). 3D-FDTD simulations show that, by considering a shift $h_b = 1\,\mu$m (this lateral shift guarantees the isolation of the drop with respect to the second resonator) and by maintaining the ratio h_b/l_b smaller than 0.2, bending losses due to radiation are negligible. On the contrary, when $h_b/l_b = 0.4$, radiation losses significantly increases, as shown in the plot reported on the bottom panel of Fig. 8. The losses are computed by comparing the transmission coefficient S_{21} of the bend with respect to the one obtained for a straight waveguide.

Simulations on a *S-bend* with a sinusoidal profile have shown that, by keeping the double curvature sufficiently smooth, it is possible to design lossless bend. For a lateral shift $h_b = 1\,\mu$m, the length of the double bend should be not smaller than $l_b = h_b/0.2 = 5\,\mu$m. With these parameters, the footprint of the *S-bend* is $5\,\mu\text{m}^2$.

2.5 Design of the mirror

The mirror is introduced at the termination of the drop waveguide close to the resonator (see Fig. 1), and is built through a series of N_m holes drilled in the *InP* photonic wire. These holes have constant radius r_m and equal distance Λ_m, except for the ones belonging to a tapering region (N_t) located at the beginning of the mirror. As described in Velha et al. (2006), the use of the taper reduces radiation losses at the waveguide-mirror interface and increases the reflectivity of the device. A sketch of the structure is illustrated in the top panel of Fig. 9. Also this component has been optimized through the computation of its transmission and reflection coefficients. The design of the mirror will be illustrated in Sect. 3.1, as the different parameters of this component can be identified only once determined the width of the drop waveguide.

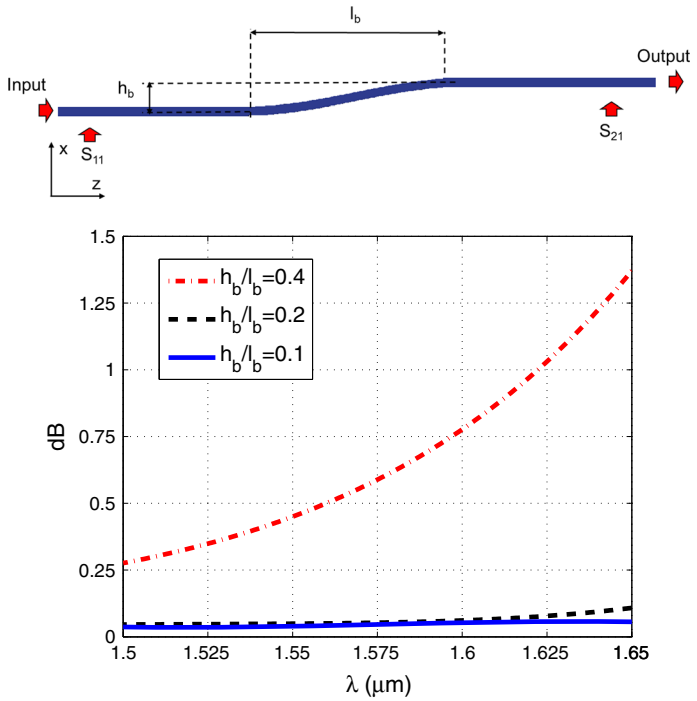

Fig. 8 *Top* sketch of the *S-bend* on the drop *InP* photonic wire waveguide with the definition of the ports for the evaluation of the transmission coefficient (S_{21}). The geometrical parameters l_b and h_b are highlighted as well. *Bottom* bending losses as a function of the wavelength for different values of the h_b/l_b ratio. *Continuous blue curve* weak curvature $h_b/l_b = 0.1$; radiation losses are negligible. *Dash-dotted dark curve* $h_b/l_b = 0.2$ medium curvature; losses due to bending are very low. *Red dashed curve* $h_b/l_b = 0.4$ tight curvature; in this case, radiation losses due to bending for longer wavelengths significantly increase. (Color figure online)

3 Design of the 3 port filters

The channel drop filter can now be built by assembling the previously described components. As anticipated in the introduction, two different configurations have been examined. The former is based on a single resonator set-up. The latter, on the contrary, exploits a double cavity system and takes advantage of the resonant-tunneling reflection-feedback effects to maximize the drop efficiency of the filter (Ren et al. 2006; Manolatou et al. 1999). The configurations of these devices and the obtained results are presented in the following sections.

3.1 Filter exploiting a single cavity configuration

The top view of the three-port single resonator drop filter is illustrated in Fig. 1. As previously stated, the maximum expected drop efficiency for this configuration is $\eta_d = 50\,\%$ (Ren et al. 2006). For this filter, actually, no power recycling could take place on the bus waveguie if only a single-mode standing-wave resonator is used. However, also if a maximum drop efficiency of 50 % can be obtained, this configuration is interesting as it is simpler to design, to tune and to fabricate respect to other possible more complex solutions.

As shown in Sects. 2.2 and 2.3, the thickness l of the SiO_2 buffer layer grown above the BCB affects the quality factor of the resonator when it is coupled with the bus (Q_b), whereas

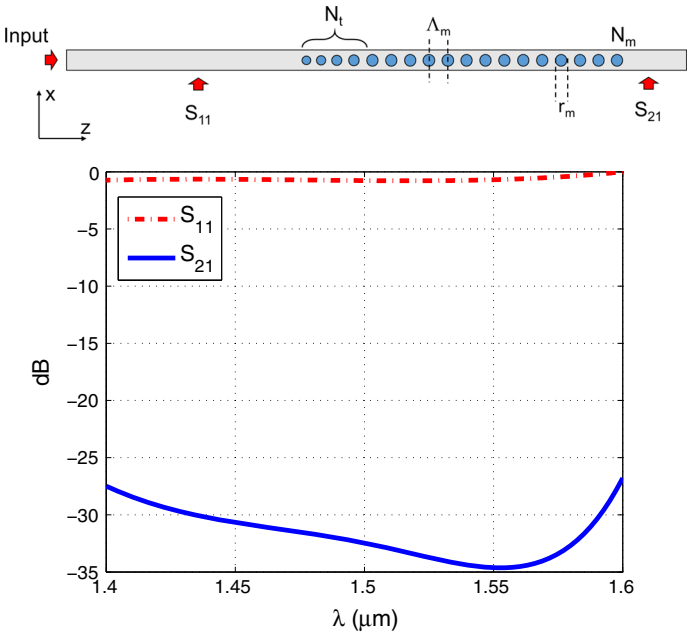

Fig. 9 *Top* sketch of the structure used for the design of the mirror with the definition of the ports for the computation of the S parameters. *Bottom* transmission (S_{21}, *continuous blue line*) and reflection (S_{11}, *dash-dotted red line*) coefficients as a function of the wavelength. (Color figure online)

the width of the drop waveguide w_d allows the tuning of the quality factor when the cavity is coupled with the drop (Q_d). Taking into account that: (i) the total quality factor of the resonator Q (and therefore the linewidth of the filter) is determined by both Q_b and Q_d; (ii) to maximize the drop efficiency $Q_b/Q_d = 2$ (Ren et al. 2006); it is clear that l and w_d cannot be chosen independently. In our design, the thickness of the SiO_2 buffer layer has been set to $l = 350\,\text{nm}$ ($Q_b = 2{,}200$). To fulfill the condition (ii) on the ratio of the quality factors, on the contrary, the width of the drop has then been set to $w_d = 425\,\text{nm}$ which gives, according to the plot of Fig. 7, $Q_d = 1{,}400$.

As the width of the drop waveguide has been optimized, it is now possible to proceed with the design of the mirror. This component has been designed and optimized by computing the transmission through a *InP* photonic wire having the same dimensions of the drop and the reflective mirror positioned between the input and the output ports.

3D-FDTD simulations have shown that $N_m = 19$ holes guarantee the building of an effective device. In the proposed design, the tapering region consists of $N_t = 4$ holes. In this region, both the radius and the period change with a parabolic profile from the minimum values of $r_{min} = 100\,\text{nm}$ and $\Lambda_{min} = 365\,\text{nm}$ to the asymptotic values of $r_m = 133\,\text{nm}$ and $\Lambda_m = 425\,\text{nm}$. The S coefficients obtained with these parameters are shown in the bottom panel of Fig. 9. As one can observe, the reflectivity in the C-band is very close to 100 % and the transmission through the mirror is roughly 30 dB below the level of the incident power. The position of the mirror with respect to the center of the Fabry–Perot cavity must also be optimized by tuning the value of the parameter d_m (distance between the initial section of the mirror and the center of the resonant cavity), in order to provide the correct phase of the reflected signal and to raise the drop efficiency of the device.

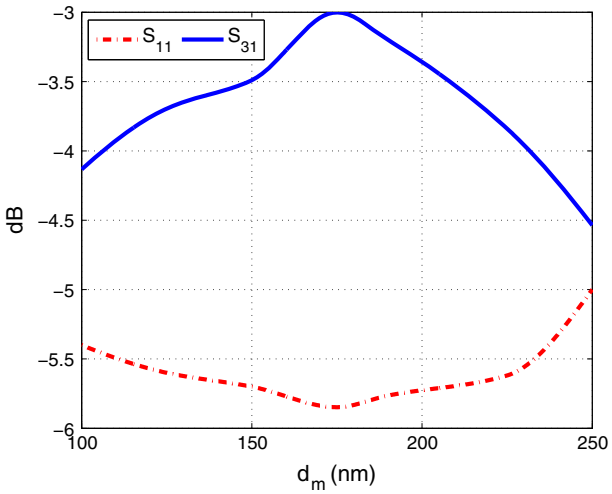

Fig. 10 Reflection coefficient at the input port (S_{11}, *dash-dotted line*) and transmission through the drop (S_{31}, *continuous blue line*) at the resonance as a function of the distance d_m between the initial section of the mirror and the center of the resonator. $d_m = 175$ nm is the optimized distance to have, for this configuration of the filter, the highest drop efficiency and the lowest reflection at the input port. (Color figure online)

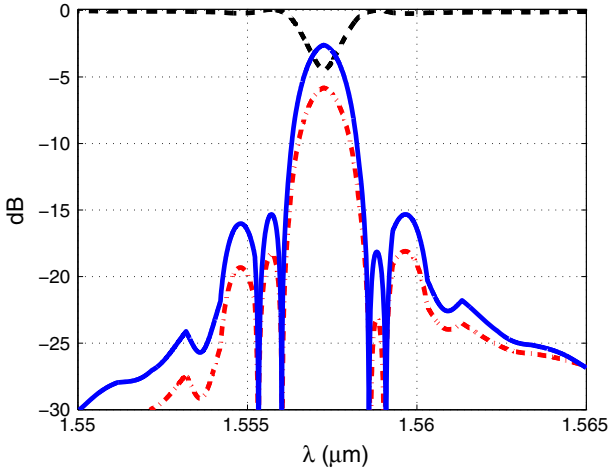

Fig. 11 *S* parameters for the single-cavity filter configuration. *Red dash-dotted line* (S_{11}): reflection at the input port. *Black dashed line* (S_{21}): transmission between the input and the output port on the bus waveguide. *Blue line* (S_{31}): transmission between the input and the output port on the drop waveguide. (Color figure online)

The influence of the parameter d_m on the performance of the filter is illustrated in Fig. 10. As one can note, the maximum of the drop efficiency is obtained for $d_m = 175$ nm.

The performance of the single-cavity CDF have been evaluated by computing the *S* parameters, which represent respectively the powers reflected at the input (S_{11}) and transferred toward the bus (S_{21}) and the drop (S_{31}) ports (see Fig. 1 for details on ports definition). Results are illustrated in Fig. 11. As one can observe, at the resonance ($\lambda_0 = 1{,}558$ nm) $S_{11} = -6.00$ dB and $S_{21} = -4.52$ dB. For the same wavelength, $S_{31} = -3.00$ dB, which corresponds to a drop efficiency of 50 % (the upper limit for this configuration).

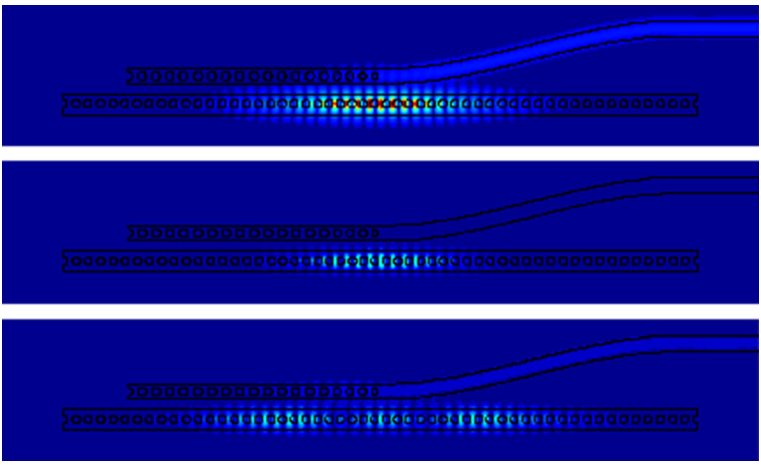

Fig. 12 Patterns of the $|E_x|$ field component. *Top* resonance on the mode with the higher Q ($\lambda = 1{,}558$ nm). The field is transferred to the drop waveguide. *Central* cavity out of resonance ($\lambda = 1{,}566$ nm). The field does not propagate on the drop waveguide. *Bottom* resonance on low Q mode ($\lambda = 1{,}612$ nm). The field on the drop waveguide has a low intensity

Table 2 Main parameters of the single cavity channel drop filter

λ(nm)	Q	$\Delta\lambda$(nm)	S_{11}(dB)	S_{21}(dB)	S_{31}(dB)
1,558	630	2.48	−6.00	−4.52	−3.00

The patterns of the $|E_x|$ field component on a horizontal xz plane cutting the cavity and the drop waveguide in their central section is illustrated in Fig. 12. In the top panel, the cavity is on resonance for the mode ($\lambda = 1{,}558$ nm) with the higher Q; in this case, the field is transferred to the drop waveguide. In the central panel, on the contrary, the cavity is out of resonance ($\lambda = 1{,}566$ nm); at this wavelength, the field does not propagate on the drop waveguide. In the bottom panel the cavity is again on resonance, but for the mode with low Q ($\lambda = 1{,}612$ nm); the field on the drop waveguide has a low intensity.

The resulting FWHM linewidth of the drop curve is close to 2.48 nm, which corresponds to an estimated quality factor Q of 630, in agreement with the values of Q_b and Q_d previously obtained. Table 2 summarizes the main parameters of the single-channel drop filter.

3.2 Filter exploiting a double cavity configuration

To constructively exploit the reflection-feedback effect, a second cavity should be correctly positioned respect to the first resonator. This cavity must be coupled with the bus waveguide, but not with the drop one: the *S-bend* on the drop makes this possible without introducing any other modifications with respect to the previously investigated design. A schematic representation of the new topology is shown in Fig. 13.

The analysis based on a coupled mode theory (CMT) approach detailed in Ren et al. (2006) and Manolatou et al. (1999) shows that, to maximize the drop efficiency of the filter, two conditions must be fulfilled: (i) to eliminate by destructive interference the portion of the signal propagating from the first cavity back toward the input, the distance L between the two resonators should verify the condition $\phi = 2\beta L = (2m + 1)\pi$, where β is the

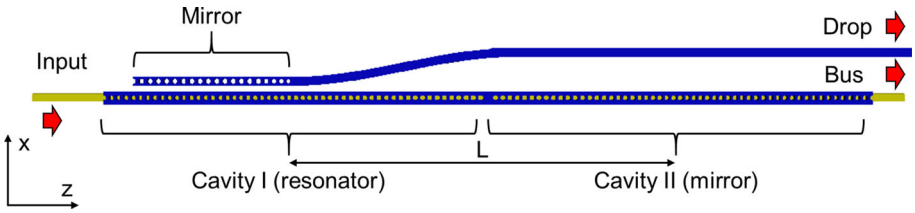

Fig. 13 *Top view* of the filter exploiting a double cavity configuration. Cavity I is the resonator whereas Cavity II acts as a mirror. L is the distance between the centers of the two resonators

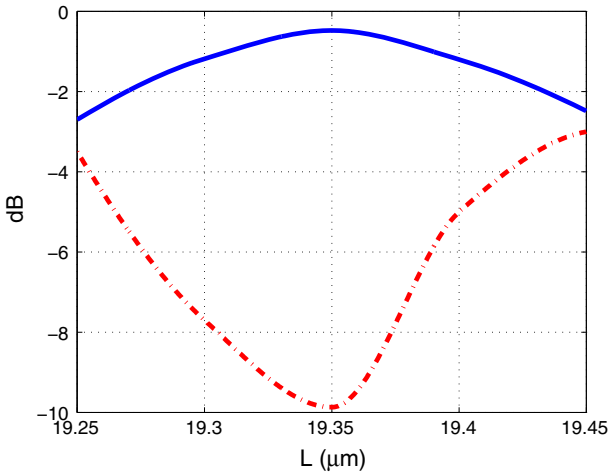

Fig. 14 S_{11} (*red dash-dotted line*) and S_{31} (*blue continuous line*) at the resonance ($\lambda = 1{,}558$ nm) as a function of the distance L between the two cavities. $L = 19.350\,\mu$m is the optimized distance that guarantees, through the reflection feedback effect provided by the mirror cavity introduced in the design, the highest drop efficiency and lowest reflection at the input port. (Color figure online)

propagation constant of the *Si* photonic wire of the bus waveguide and m is an integer; (ii) to maximize the transfer to the drop, $Q_b/Q_d = 2$, being Q_b and Q_d the previously defined quality factors of the first cavity. Due to the fact that the design of the device with a single resonator complies with the condition relevant to the ratio of the Qs, here we focus our attention on the optimization of the distance L between the resonators. This parameter has been tuned through 3D-FDTD simulations.

Figure 14 shows how L influences S_{11} and S_{31}. From this analysis we obtained that $L = 19.350\,\mu$m optimizes the performance of the filter. For the topology with the double-cavity, modifications of L strongly affect both the drop (S_{31}) and the reflection (S_{11}) coefficients. In fact, only when the mirror resonator (Cavity II) is out of phase respect to the output one (Cavity I), the reflections from the two cavities coupled to the bus waveguide add destructively and effectively leads to zero the back reflection. This condition also enhance the amount of power transferred to the drop, thus increasing the output efficiency on this port.

The S parameters in Fig. 15 illustrates the performance of the double-cavity channel drop filter (see Fig. 13 for details on ports definition). At the resonance ($\lambda_0 = 1{,}558$ nm) $S_{11} = -10.00$ dB and $S_{21} = -14.50$ dB. For the same wavelength, $S_{31} = -0.40$ dB, which corresponds to a drop efficiency of 91.2 %. Also for this topology, a drop efficiency very close to the upper theoretical limit has been reached.

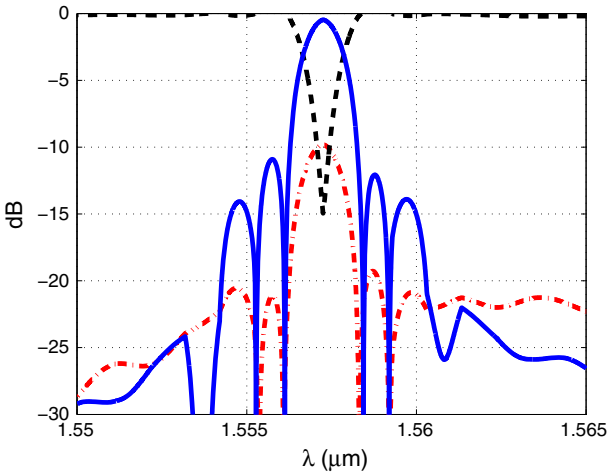

Fig. 15 S parameters for the double-cavity filter configuration. *Red dash-dotted line* (S_{11}): reflection at the input port. *Black dashed line* (S_{21}): transmission between the input and the output port on the bus waveguide. *Blue line* (S_{31}): transmission between the input and the output port on the drop waveguide. (Color figure online)

Table 3 Main parameters of the double-cavity channel drop filter

λ(nm)	Q	Δλ(nm)	S_{11}(dB)	S_{21}(dB)	S_{31}(dB)
1,558	1,200	1.27	−10.00	−14.50	−0.40

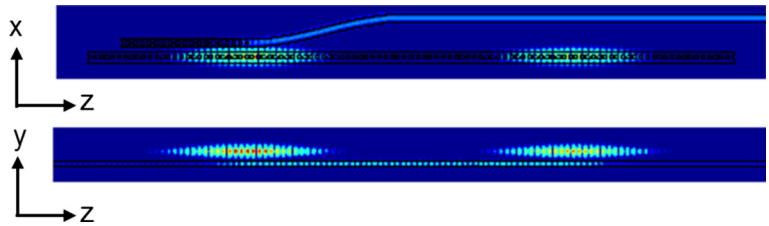

Fig. 16 Pattern of the $|\ E_x\ |$ field component at the resonance ($\lambda = 1{,}558$ nm) on a horizontal xz plane (*top panel*) intersecting the cavities and on a vertical yz plane (*bottom panel*) through the cavities and the bus waveguide. As can be observed in the *top figure*, both the cavities resonate and the field is efficiently transferred to the drop waveguide. On the *bottom figure*, the standing wave in the bus waveguide in the region between the two resonators is clearly visible

The resulting FWHM linewidth of the drop curve is close to 1.27 nm, which corresponds to an estimated quality factor Q of about 1,200. Table 3 summarizes the parameter of the double-channel drop filter.

The patterns of the $|\ E_x\ |$ field component at the resonance wavelength of the filter ($\lambda = 1{,}558$ nm) are reported in Fig. 16. The top panel refers to a horizontal xz plane intersecting the cavities and the drop waveguide. The two cavities are both on resonance, and the field is efficiently transferred by the first resonator to the drop waveguide. The bottom panel, shows the field intensity on a vertical yz plane across the cavities and the bus waveguide. In this case it is interesting to note the standing wave pattern located between the two resonators. This standing wave is generated by the field propagating from Cavity I to Cavity II and

reflected by Cavity II toward Cavity I. As the correct phase relation is verified, there is no field propagating back to the input port. Moreover, due to the high drop efficiency, also the field in propagation on the bus after the second resonator is not visible, due to its low intensity.

4 Conclusions

In this paper, two different configurations of a three-port channel drop filter for the C-band (1,550 nm) on a hybrid III/V semiconductor/silicon have been described by using simulation results. After a short introduction, the design and the optimization procedures of all the different components used for these devices have been presented. In the first configuration, which uses a single Fabry–Perot resonator, the theoretical drop efficiency of 50 % and a filter bandwidth of about 2 nm have been obtained. To increase the drop efficiency, a different design based on a two-cavity configuration has then been investigated. With this new topology, a drop efficiency close to 100 %, and a bandwidth of about 1.3 nm, have been reported.

Acknowledgments The authors acknowledge funding from the EC under the project Copernicus (249012).

References

Ahn, B.H., Kang, J.H., Kim, M.K., Song, J.H., Min, B., Kim, K.S., Lee, Y.H.: One-dimensional parabolic-beam photonic crystal laser. Opt. Express **18**(6), 5654660 (2010)

Carette, M., Vilcot, J.P., Bernard, D., Decoster, D.: InP/benzocyclobutene optical nanowires. Electron. Lett. **44**, 902–904 (2008)

Chao, C., Li, X., Li, H., Xu, K., Wu, J., Lin, J.: Bandpass filters based on phase-shifted photonic crystal waveguide gratings. Opt. Express **15**, 11278–11284 (2007)

Combrié, S., Lehoucq, G., Junay, A., Malaguti, S., Bellanca, G., Trillo, S., Menager, L., Reithmaier, J.-P., De Rossi, A.: All-optical signal processing at 10 GHz using a photonic crystal molecule. Appl. Phys. Lett. **103**, 193510 (2013)

Deotare, P.B., McCutcheon, M.W., Frank, I.W., Khan, M., Lončar, M.: High quality factor photonic crystal nanobeam cavities. Appl. Phys. Lett. **94**(12), 121106 (2009)

Frear, D.R.: Materials issues in area-array microelectronic packaging. JOM **51**, 22–27 (1999)

Halioua, Y., Bazin, A., Monnier, P., Karle, T.J., Sagnes, I., Roelkens, G., Van Thourhout, D., Raineri, F., Raj, R.: III–V photonic crystal wire cavity laser on silicon wafer. J. Opt. Soc. Am. B **27**(10), 2146150 (2010)

Halioua, Y., Bazin, A., Monnier, P., Karle, T., Roelkens, G., Sagnes, I., Raj, R., Raineri, F.: Hybrid III–V semiconducto/silicon nanolaser. Opt. Express **19**, 9221–9231 (2011)

Haus, H.A., Lai, Y.: Narrow-band distributed feedback reflector design. IEEE J. Lightwave Technol. **9**(6), 754–760 (1991)

Haus, H.A., Lai, Y.: Narrow-band optical channel-dropping filter. IEEE J. Lightwave Technol. **10**(1), 57–62 (1992)

Kane, C.F., Krchnavek, R.R.: BenzoCyclobutene Optical Waveguides. IEEE Photon. Technol. Lett. **7**, 535–537 (1995)

Liu, Y.S., Cole, H.S., Bristow, J., Yue, Liu.: Polymer-based optical interconnect technology—a route to low-cost optoelectronic packaging and interconnect. In: Proceedings of SPIE 2400, Optoelectronic Interconnects III, 80, 5 April 1995

Malaguti, S., Bellanca, G., Ottaviano, L., Yvind, K., Combrié, S., De Rossi, A., Trillo, S.: Tailored design of WDM filters in BCB embedded PhC membranes. Opt. Quantum Electron. **45**, 329–342 (2013)

Manolatou, C., Khan, M.J., Fan, S., Villeneuve, P.R., Haus, H.A., Joannopoulos, J.D.: Coupling of modes analysis of resonant channel add-drop filters. IEEE J. Quantum Electron. **35**, 1322–1331 (1999)

Nguyen, T.N., Gay, M., Lenglé, K., Bramerie, L., Thual, M., Simon, J.C., Malaguti, S., Bellanca, G., Trillo, S., Combrié, S., Lehoucq, G., De Rossi, A.: 100-Gb/s wavelength division demultiplexing using a photonic crystal four-channel drop filter. IEEE Photon. Techlog. Lett. **25**, 813–816 (2013)

Niemi, T., Frandsen, L.H., Hede, K., Harpoth, A., Borel, P.I., Kristensen, M.: Wavelength-division demultiplexing using photonic crystal waveguides. IEEE Photon. Technol. Lett. **18**, 226–228 (2006)

Notomi, M.: Manipulating light with strongly modulated photonic crystals. Rep. Prog. Phys. **73**, 096501 (2010)

Park, H., Fang, A., Cohen, O., Jones, R., Paniccia, M., Bowers, J.: A hybrid AlGaInAs-silicon evanescent amplifier. IEEE Photon. Technol. Lett. **19**, 230–232 (2007)

Qiang, Z., Zhou, W., Soref, R.A.: Optical add-drop filters based on photonic crystal ring resonators. Opt. Express **15**, 1823–1831 (2007)

Ren, H., Jiang, C., Hu, W., Gao, M., Wang, J.: Photonic crystal channel drop filter with a wavelength-selective reflection micro-cavity. Opt. Express **14**, 2446–2458 (2006)

Shinya, A., Mitsugi, S., Kuramochi, E., Notomi, M.: Ultrasmall multi-port channel drop filter in two-dimensional photonic crystal on silicon-on-insulator substrate. Opt. Express **14**, 12394–12400 (2006)

Van Campenhout, J., Romeo, P., Regreny, P., Seassal, C., Van Thourhout, D., Di Cioccio, L., Fedeli, J.M., Baets, R.: Electrically pumped InP-based microdisk lasers integrated with a nanophotonic silicon-on-insulator waveguide circuit. Opt. Express **15**, 6744–6749 (2007)

Van Thourhout, D., Spuesens, T., Selvaraja, S., Liu, L., Roelkens, G., Kumar, R., Morthier, G., Rojo-Romeo, P., Mandorlo, F., Regreny, P., Raz, O., Kopp, C., Grenouillet, L.: Nanophotonic devices for optical interconnect. IEEE J. Sel. Top. Quantum Electron. **16**, 1363–1375 (2010)

Veerasubramanian, V., Beaudin, G., Giguère, A., Le Drogoff, B., Aimez, V., Kirk, A.G.: Waveguide-coupled drop filters on SOI using quarter-wave shifted sidewalled grating resonators. Opt. Express **20**, 15983–15990 (2012)

Velha, P., Rodier, J.C., Lalanne, P., Hugonin, J.P., Peyrade, D., Picard, E., Charvolin, T., Hadji, E.: Ultra-high-reflectivity photonic-bandgap mirrors in a ridge SOI waveguide. N. J. Phys. **8**, 1–13 (2006)

Wang, C.C., Chen, L.W.: Channel drop filters with folded directional couplers in two-dimensional photonic crystals. Phys. B **405**, 1210–1215 (2010)

Zain, A.R.M., Johnson, N.P., Sorel, M., De La Rue, R.M.: Ultra high quality factor one dimensional photonic crystal/photonic wire micro-cavities in silicon-on-insulator (SOI). Opt. Express **16**, 12084–12089 (2008)

Zhang, Y., Khan, M., Huang, Y., Ryou, J., Deotare, P., Dupuis, R., Lončar, M.: Photonic crystal nanobeam lasers. Appl. Phys. Lett. **97**(5), 051104 (2010)

Zheng, J.F., Hanberg, J., Demir, H.V., Sabnis, V.A., Fidaner, O., Harris, J.S., Miller, D.A.B.: Novel planarization and passivation in the integration of III–V semiconductor devices. Proc. SPIE **535**, 81–91 (2004)